

# Polarization Signatures of Frozen and Thawed Forests of Varying Environmental State

Ronald Kwok, *Member, IEEE*, Eric J. M. Rignot, *Member, IEEE*, JoBea Way, Anthony Freeman, *Member, IEEE*, and John Holt

**Abstract**—During the two different overflights of the Bonanza Creek Experimental Forest (near Fairbanks, Alaska) by the NASA/JPL radar polarimeter in March 1988, the environmental conditions over the region changed significantly with temperatures ranging from unseasonably warm (1 to 9°C) during one day to well below freezing (−8 to −15°C) during the other. The moisture content of the snow and trees changed from a liquid to frozen state causing significant changes in the radiometric and polarimetric responses of the forest to the radar wave. The L-band polarimetric observations are summarized in this paper. Up to a 6 dB change in the backscatter was observed in certain forest stands at L-band. Features extracted from the Stokes matrices of the same stands from the thawed and frozen days suggest the changes in the relative contribution of the different scattering mechanisms to the radar return. Comparison of the polarimetric signatures indicate relatively higher contribution from diffuse scatterers on the thawed day than on the frozen day. The sensitivity of the polarimetric signatures to changing environmental conditions is clearly demonstrated.

## I. INTRODUCTION

IN March 1988, the NASA/JPL Airborne Synthetic Aperture Radar (AIRSAR) acquired a series of imaging radar datasets over the Bonanza Creek Experimental Forest (BCEF) near Fairbanks, Alaska. The P-, L-, and C-band polarimetric datasets consist of data collected on five different days over a period of two weeks. During that period, the environmental conditions over the region changed significantly with temperatures ranging from unseasonably warm (1 to 9°C) on March 13 to well below freezing (−8 to −15°C) on March 19 [1]. The changes in the water status of the snow and trees from a liquid to frozen state caused significant changes in the backscatter characteristics of the forest. The changes in the microwave properties of the forest during the two data acquisition flights (March 13 and 19) over the BCEF offered an opportunity for comparison of scattering characteristics of forest stands in different temperature regimes, thus providing physical insights into the contribution of different scattering mechanisms to the observed radar return on the cold and warm days. The synthesized total power (L-band)

Manuscript received February 1991; revised November 24, 1993. This work was supported by the National Aeronautics and Space Administration at the Jet Propulsion Laboratory, California Institute of Technology.

R. Kwok, E. Rignot, J.-B. Way, and A. Freeman are with Jet Propulsion Laboratory, California Institute of Technology, Pasadena, CA 91109.

J. Holt is with the Department of Geology, California Institute of Technology, Pasadena, CA, 91125.

IEEE Log Number 9215448.



Fig. 1. L-band total power images of the Bonanza Creek area. (a) From March 13. (b) From March 19.

images for both days are shown in Fig. 1. The radiometric differences are easily observable. These dramatic changes in the scattering signature have been reported in a preliminary paper by Way *et al.* [1]. The purpose of this paper is to present the quantitative radar measurements of these changes based on radiometrically and polarimetrically calibrated data with an emphasis on the polarimetric signatures. Results from microwave backscattering modeling have been reported by Dobson *et al.* [3]. Applications of their technique to the monitoring of growing season length was reported by Way *et al.* [11].

This paper is organized as follows. Brief descriptions of the field experiment, the airborne SAR dataset, and the calibration of the data are given in Section II. The forest sites which were selected for study are described in Section III. Section IV examines the radiometric and polarimetric characteristics of the different forest stands. The interpretation of these signatures is discussed based on previous observations and modeling work [3]. Conclusions are provided in Section V.

## II. RADAR DATASET

This section provides a brief description of the airborne SAR dataset, the Alaska field experiment, and the calibration of the dataset.

### Airborne SAR Data

The radar dataset was acquired by the NASA/JPL multifrequency radar polarimeter which was flown on a DC-8 aircraft. The radar operates in the C-, L-, and P-bands (0.45, 1.26, 5.31 GHz, respectively). Each frequency channel has the capability of simultaneously collecting linear like-polarized (HH and VV) and cross-polarized (HV and VH) backscatter data. The transmitter alter-

TABLE I  
NASA/JPL AIRCRAFT SAR CHARACTERISTICS

SAR Parameters	
Bands	P, L, C
Frequencies (GHz)	0.450, 1.26, 5.31
Polarization	quad
Swath (km)	7
Resolution (m)	10
Simultaneously recorded channels	12
Flight Line Parameters	
Swath center point	64° 45' N, 148° 00' W
Track length (km)	~ 70
Track heading	54° to true north
Center incidence angle	40°

TABLE II  
AIRSAR PARAMETERS AND ENVIRONMENTAL CONDITIONS AT TIME OF OVERFLIGHTS

Date (1988)	Time <sup>a</sup>	AIRSAR Channels	Incidence Angle <sup>b</sup>	Air Temperature (C)	Soil Temperature (C)	Snow Temperature (C)	Snow Moisture (%vol)	Snow Upper Layer Condition	Bole Condition	Bole Maximum Real Dielectric Constant
3/11	14:02	P, L, C	9°	7.5	-2/0	0	2-5	wet	thawed	25-30
3/13	15:03	P, L <sup>c</sup>	41°	2.0	-2/0	0	5-7	wet	thawed	25-30
3/17	14:54	L, C <sup>d</sup>	40°	-13	-3/-1	-13	0	dry	frozen	5
3/19	23:17	L, C <sup>d</sup>	39°	-14	-3/-1	-12	0	dry	frozen	5
3/21	23:38	L, C <sup>d</sup>	48°	< -20	-3/-1	-30	0	dry	frozen	5

<sup>a</sup>Local Alaska time; time of overflight of BCEF.

<sup>b</sup>At center of Seven Mile Island.

<sup>c</sup>C-band data contain banding due to aircraft motion during imaging.

<sup>d</sup>H-pol transmitted only on P-band.

<sup>e</sup>At 5 cm/50 cm depth.

nately drives the horizontally and vertically polarized antennas while dual receivers simultaneously record the like-polarized and cross-polarized echoes. In this manner, the complete polarization signature of every resolution element in an image is measured. The radiometric and polarization signatures are also spatially registered. The spatial resolution (defined by the 3-dB widths of the impulse response) of the 4-look SAR data is approximately 6.6 m in the range and 11 m in the azimuth direction. The range of look angles across an image is between 20° and 70°. Table I summarizes the aircraft SAR characteristics. The data quality is discussed later in this section. For the purposes of this paper, the key dataset (explained in the following section) is the L-band polarimetric data from March 13 and 19.

#### The Alaska Field Experiment

Extensive ground data were collected during the aircraft overflights [1], [11]. Sampling of forest canopy parameters for input to microwave models and monitoring the environmental and phenologic states of the stands were emphasized. For each of the test stands identified for the BCEF, ancillary data which consisted of relatively static site descriptors (i.e., species composition, stand height,

diameter at breast height (DBH), and stem density) and descriptors of variable scene properties (i.e., plant water status and dielectric properties and snow pack properties including snow water equivalent, snow wetness, and dielectric constant) were collected. Tables II and III summarize the parameters of several white spruce (WS), black spruce (BS), and balsam poplar (BP) stands.

#### Environmental Conditions during March 13 and March 19

Data over the BCEF test site were acquired on five separate occasions by the JPL SAR. Overlapping passes were acquired on March 13, March 17, and March 19. Since the SAR data from March 17 and 19 (when temperatures were below freezing) are similar and there were problems with the C-band channel on March 13 and the P-band channel on March 17 and 19, only the L-band data from the March 13 and March 19 passes are considered in this paper. During the field experiment, an unusually warm period (1 to 9°) occurred in the early part of March creating unseasonably warm conditions (moist snow) and initiating thawing of the boles of the trees. By March 13, a high pressure system spreading over Alaska from the west diminished cloud cover and reduced temperatures

TABLE III  
MEASURED CANOPY PARAMETERS

Stand	Age (years)	Mean DBH (cm)	Mean Height (m)	Density (no./ha)	Winter* Biomass ( $10^3$ kg/ha)
CC-01	6	0	0	0	0
CC-02	9	0	0	0	0
BP-02	90	18.0	17.6	1615	179 (182)
BP-06	30	7.3	9.1	3699	34 (36)
BP-13	75 est	18.5	15.2	1125	104 (106)
WS-01	165	19.6	22.1	1248	217
WS-02	100	14.5	20.1	2073	167
WS-04	124	25.0	22.0	608	163
WS-05	180	17.9	21.3	1484	181
BS-01	200	8.8	7.6	1975	37
BS-02	200	8.2	6.8	1402	23

\*Note: Summer biomass values for balsam poplar and white spruce are shown in parentheses.

slightly. A weather front from the south produced light snow and lowered temperatures on March 17; the effect of the front diminished on March 18. Low pressure in the Gulf of Alaska on March 19 brought moisture northward, again producing light snow and bringing subfreezing temperatures. The characteristics of the local weather during the time of the two overflights are shown in Table II. A detailed description of the meteorological conditions can be found in [1].

#### L-Band Data Calibration

The calibration procedure for this polarimetric radar dataset was reported by Holt and Freeman [2], in which an algorithm developed by Klein [4] was used. This algorithm is based on the assumptions that the HV and VH backscatter are reciprocal, that the HH and HV returns from natural targets are uncorrelated, and that the radar is stable within an image and between images collected within a few minutes of each other. The calibration procedure first removes the crosstalk between the radar channels, corrects the relative amplitude and phase balances between polarizations, and then adjusts the absolute gain of the radar data. A trihedral corner reflector response is required to complete the calibration.

At BCEF, there were no suitable trihedral corner reflectors available within the imaged scene. Instead, measurements were made on a set of trihedrals deployed at the Fairbanks airport, 24-km down-track of BCEF. For these measurements to be valid for calibrating the BCEF scene, the radar must be stable for the time taken to collect data over the two areas. To verify this, we examined the average HV/VH backscatter ratio for each scene on the two days and found that it varied by less than 0.1 dB in amplitude and  $2^\circ$  in phase between the two sites on any given day. We also examined both the Fairbanks and BCEF images after calibration. Backscatter ( $\sigma_0$ ) values from patches of river ice and marsh, viewed at similar incidence angles, were extracted. We found that the HH and HV backscatter varied by less than 0.6 dB between scenes.

TABLE IV  
CALIBRATION UNCERTAINTY ESTIMATES

Long-term relative (day-to-day)	$\pm 1.9$ dB
Short-term relative (scene-to-scene)	$\pm 0.6$ dB
Short-term relative (across scene)	$\pm 0.6$ dB
Polarimetric amplitude balance	$\leq 0.1$ dB
HH/VV phase imbalance	$\pm 5^\circ$
HV/VH phase imbalance	$\pm 5^\circ$
Polarimetric crosstalk	$\leq -2.5$ dB

Calibration uncertainty estimates for the BCEF (and Fairbanks) scenes are summarized in Table IV. The long and short-term relative uncertainties were estimated from results obtained at the Goldstone calibration site [2]. These uncertainties represent the limits of sensitivity of the radar measurements: for example, a change in the HH/VV phase difference must be greater than  $1.5^\circ$  to be regarded as significant.

### III. SITE SELECTION FOR COMPARISON OF RADAR SIGNATURES

A total of 35 test sites within BCEF were selected for radar signature comparison purposes. The locations of these stands are shown in Fig. 2. Included were 24 forest stands which consisted of 11 white spruce (WS) stands, 5 black spruce (BS) stands, 7 balsam poplar (BP) stands, and 1 mixed white spruce/balsam poplar (WSBP) stand. Sample photographs of these three forest stands are shown in Fig. 3. Ten other areas including 2 clear-cut (CC) sites, 3 sandbar (SB) sites, and 2 bog (BG) sites were also selected. More detailed descriptions of the stand characteristics can be found in [1], [11]. The radar signatures from the nonforested areas provide us with a measure of the magnitude of the changes compared to the forested areas. All of the stands are on the flat areas along the Tanana River to avoid the effects of topography on local incidence angle. The window size selected for sampling the radar measurements is  $25 \times 25$  pixels or approximately  $0.6 \text{ km}^2$  in area. The data windows are located within a narrow range of incidence angles (between  $40^\circ$  and  $50^\circ$ ), so the dependence of the radar measurements on the incidence angle is reduced. Within each of the stands, the average variation of the backscatter (Tables V and VI) is usually less than 1 dB.

### IV. POLARIMETRIC SAR OBSERVATIONS—FROZEN AND THAWED FOREST STANDS

This section presents and summarizes the changes in the polarimetric behavior of the sites described in the previous section. To reduce the large data volume generated by the radar, the polarimetric data currently distributed by JPL are stored in the compressed Stokes matrix format [5]. From the decoded Stokes matrix data, the polarization signature of a given sample window can be reconstructed or synthesized [6]. In this paper, all scattering signatures whether polarimetric or radiometric are derived in this manner. We usually use "polarimetric" to refer to

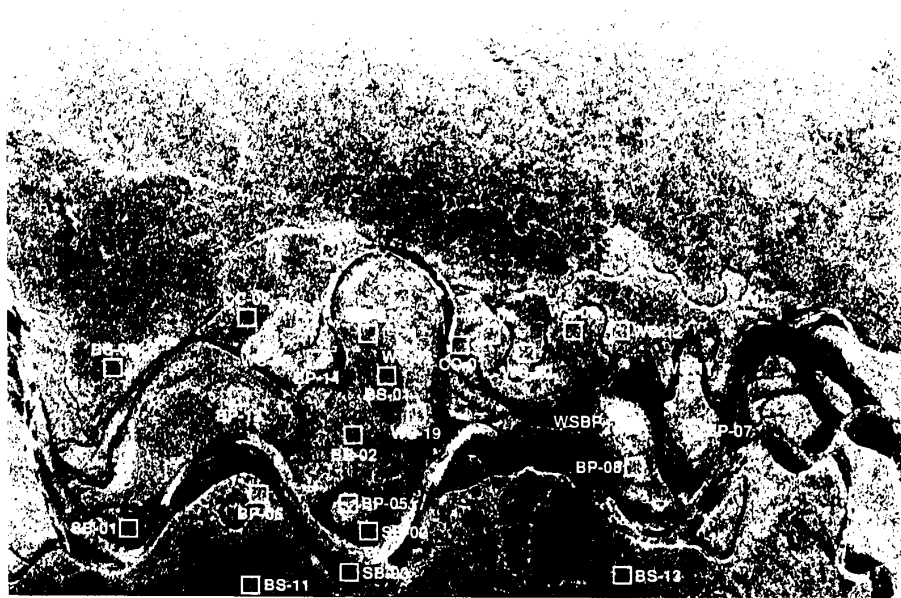


Fig. 2. Location of test sites (WS: White Spruce, BS: Black Spruce, BP: Balsam Poplar, CC: Clear Cut, SB: Sand Bar, BG: Bog, WSBP: White Spruce/Balsam Poplar).

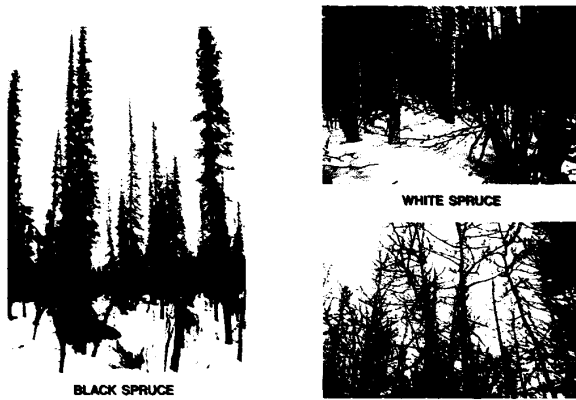


Fig. 3. Typical White Spruce, Black Spruce, and Balsam Poplar stands.

signatures where the relative phase between the radar channels is involved and “radiometric” to refer to single channel signatures. Sample signatures extracted from different test sites (balsam poplar, white spruce, black spruce, bog, sand bar, clear-cut) from the warm and cold days are shown in Fig. 4; the plots are normalized (to the total power) three-dimensional representations of the copolarized and cross-polarized radar backscatter at a given incidence angle. These signatures were created by averaging a  $25 \times 25$  area of 4-look pixels. Copolarized signatures are obtained by setting the receive polarization of the antenna equal to that transmitted and by calculating

TABLE V  
BONANZA CREEK FOREST EXPERIMENT (March 13th 1988)  
L-BAND MEASUREMENTS

Site	$\sigma_0^{HH}$	$\sigma_0^{HV}$	$\sigma_0^{VV}$	$r_{HHVV}$	$\phi_{HV}$	$\Delta\phi_{HV}$	$f_p$
WS-01	-8.0	-13.8	-9.5	1.5	-2.2	82.4	0.57
WS-02	-8.4	-14.5	-9.7	1.3	-7.9	86.2	0.61
WS-03	-9.2	-14.6	-9.6	0.4	-12.0	71.5	0.54
WS-04	-9.3	-14.2	-9.4	0.1	-0.9	81.7	0.51
WS-05	-7.9	-14.0	-9.0	1.1	-10.7	83.6	0.58
WS-06	-8.1	-13.7	-8.8	0.7	-5.5	69.9	0.56
WS-12	-8.8	-14.3	-9.3	0.5	-14.2	76.5	0.57
WS-17	-8.7	-14.0	-9.6	0.9	0.0	78.7	0.54
WS-19	-8.9	-15.2	-10.5	1.6	4.4	80.4	0.59
WS-20	-8.8	-13.8	-8.8	0.0	-3.1	80.7	0.52
WS-22	-7.8	-14.4	-10.2	2.4	-7.8	80.6	0.62
WSBP2	-6.8	-14.2	-9.5	2.7	-6.5	104.6	0.5
BS-01	-13.4	-20.1	-14.7	1.3	-1.9	62.8	0.65
BS-02	-12.3	-19.2	-14.0	1.7	-12.0	66.5	0.63
BS-06	-14.1	-21.3	-15.5	1.4	-10.6	53.3	0.66
BS-11	-12.8	-20.5	-14.9	2.1	-6.0	72.8	0.69
BS-13	-12.2	-18.3	-13.5	1.3	0.7	72.8	0.60
BP-02	-8.9	-14.1	-10.2	1.3	-11.3	82.7	0.53
BP-05	-8.6	-14.0	-10.0	1.4	-6.1	88.5	0.54
BP-06	-8.7	-13.7	-9.8	1.1	2.0	88.5	0.52
BP-07	-8.9	-13.9	-9.8	0.9	-9.8	86.7	0.50
BP-08	-8.6	-13.7	-9.7	1.1	-9.4	82.1	0.50
BP-13	-7.9	-13.7	-10.0	2.1	-11.9	81.2	0.57
BP-14	-8.2	-13.6	-9.4	1.2	-18.0	82.5	0.54
CC-01	-14.5	-24.3	-15.4	0.9	-14.7	42.1	0.76
CC-02	-14.5	-25.1	-15.1	0.6	-2.3	31.6	0.81
SB-01	-20.0	-30.5	-19.6	-0.4	-1.2	32.6	0.87
SB-02	-18.1	-25.3	-17.9	-0.2	-14.5	48.6	0.78
SB-03	-15.2	-22.6	-15.2	0.0	-15.4	80.2	0.71
BG-01	-11.8	-21.5	-12.2	0.4	3.8	28.8	0.79

Note: WS: White Spruce; BP: Balsam Poplar; CC: Clear Cut; BS: Black Spruce; SB: Sand bar; BG: Bog; WSBP: White Spruce/Balsam Poplar mixture.

TABLE VI  
BONANZA CREEK FOREST EXPERIMENT (March 19th 1988)  
L-BAND MEASUREMENTS

Site	$\sigma_0^{HH}$	$\sigma_0^{HV}$	$\sigma_0^{VV}$	$r_{HHVV}$	$\phi_{H-V}$	$\Delta\phi_{H-V}$	$f_p$
WS-01	-11.3	-20.6	-14.6	3.3	-9.3	65.0	0.76
WS-02	-11.3	-20.8	-14.4	3.1	-15.0	65.4	0.76
WS-03	-13.5	-22.1	-15.7	2.2	-2.4	55.8	0.72
WS-04	-12.3	-20.3	-14.1	1.8	8.8	51.7	0.70
WS-05	-11.1	-21.1	-14.8	3.7	-16.0	74.0	0.79
WS-06	-12.0	-20.5	-13.9	1.5	0.6	56.9	0.73
WS-12	-12.3	-20.9	-14.5	2.2	6.2	57.7	0.73
WS-17	-11.7	-20.0	-14.2	2.5	-2.5	60.5	0.72
WS-19	-11.8	-20.8	-14.8	3.0	-4.3	78.6	0.71
WS-20	-12.0	-20.1	-13.5	1.5	5.3	51.9	0.76
WS-22	-11.5	-20.8	-15.5	4.0	-15.5	66.3	0.78
WSBP2	-8.6	-19.1	-13.9	5.3	-33.9	93.1	0.73
BS-01	-15.1	-24.9	-16.6	1.5	3.4	40.5	0.76
BS-02	-14.7	-23.7	-16.7	2.0	5.9	48.1	0.80
BS-06	-14.8	-24.8	-16.2	1.4	6.0	35.8	0.78
BS-11	-14.8	-24.6	-18.2	3.4	5.5	60.1	0.76
BS-13	-14.1	-23.5	-16.1	2.0	4.2	49.3	0.72
BP-02	-12.5	-21.0	-14.6	2.1	-9.2	54.0	0.73
BP-05	-11.8	-20.6	-15.0	3.2	-9.3	69.3	0.74
BP-06	-12.7	-21.3	-15.9	3.2	0.2	74.1	0.71
BP-07	-11.5	-19.6	-14.2	2.7	-7.5	76.4	0.68
BP-08	-12.0	-19.8	-14.4	2.4	-1.3	59.4	0.78
BP-13	-11.4	-21.2	-15.6	4.2	-13.3	64.0	0.72
BP-14	-11.8	-20.3	-14.9	3.1	-5.4	67.4	0.72
CC-01	-13.5	-24.9	-13.7	0.2	5.4	39.3	0.81
CC-02	-15.1	-26.1	-16.0	0.9	7.4	33.5	0.82
SB-01	-19.6	-31.7	-19.4	-0.2	3.6	31.4	0.87
SB-02	-20.0	-32.8	-19.4	-0.6	2.3	34.2	0.89
SB-03	-17.3	-29.0	-18.9	1.6	-6.3	60.1	0.86
BG-01	-13.9	-25.0	-13.7	-0.2	14.2	41.7	0.84

the backscatter response as the polarization orientation and ellipticity angles are varied [6]. Cross-polarized signatures are synthesized by setting the receive polarization of the antenna orthogonal to that of the transmitted. The signatures are composed of a variable portion which sits on top of a pedestal (this feature is discussed later). In general, the signature in the forested areas generally exhibits a higher pedestal than, for example, the clear-cut areas shown here (this effect is discussed in the following sections). The measurements extracted from the different forest stands are shown in Tables V and VI for the frozen and thawed days, respectively. The following subsections discuss some of the more salient features in the observed radar signatures of the different test sites described in the previous section. To limit the length of the paper and due to the availability of data, the emphasis of the following discussions is placed on between-date rather than between-stand comparisons at L-band.

#### Like-Pol ( $\sigma_0^{HH}$ , $\sigma_0^{VV}$ ) and Cross-Pol Backscatter ( $\sigma_0^{HV}$ ): L-Band

Fig. 5(a) and 5(b) summarizes the dramatic differences in the L-band copolarized and cross-polarized backscatter signatures between the warm day (3/13) and the cold day (3/19). The observed changes are significant compared to the calibration uncertainties given in Table IV. On the

warm day, the radar backscatter was higher in all three types of forest stands selected. On March 19, when the water in both the snow and the trees was frozen and the dielectric constants were low, the backscatter at all polarizations decreased significantly. This demonstrates the sensitivity of the backscatter to the environmental conditions; the decrease in the dielectric constant of the forest canopy results in a decrease in the contribution of diffuse scatterers [2]. Typically, the expected return from forested areas is slightly greater at horizontal polarization than that at vertical polarization [7] and this is observed in the data collected during both days. This phenomenon is usually attributed to branch and ground-trunk scattering from the canopy [7]. Also, note that the decrease in the VV-responses ( $\sim 5$  dB) are much greater than the HH-responses ( $\sim 3$  dB) between the thawed and frozen days. The trend could be observed in the ratio of the HH- to VV- responses ( $r_{HHVV}$ ) in Tables V and VI. The changes in the cross-pol backscatter between the two dates are shown in Fig. 5(b). By comparison, there is relatively little change in the cross-pol returns from the unforested areas (e.g., sand bars, clear cuts). These two observations could be explained by decreases in the relative contribution of branch scattering and increases in the relative contribution of direct returns from the ground on the cold day (when the V-return usually dominates for surface scattering). This observation is confirmed by other measurements discussed in the following sections.

#### Fractional Polarization $f_p$ , Polarimetric Phase $\phi_{H-V}$ Distribution: L-Band

Two other measurements extracted from the Stokes matrices of these forest stands are the fractional polarization ( $f_p$ ) and H-V phase difference ( $\phi_{H-V}$ ) distribution or polarimetric phase distribution. The fractional polarization  $f_p$  is defined as [6], [7]:

$$f_p = \frac{P_{\max} - P_{\min}}{P_{\max} + P_{\min}}$$

where  $P_{\min}$  and  $P_{\max}$  are the minimum and maximum powers over both the copolarization and cross-polarization signatures, respectively. When  $f_p = 1$ , the average return is completely polarized and variations in antenna polarization (receive and transmit) will cause relatively large changes in the average backscattered power. When  $f_p = 0$ , the average return is completely unpolarized, and variations in antenna polarization will not change the average backscatter power. In general, the larger the  $f_p$ , the greater the amount of polarized power in the average return. It can be seen (Fig. 4) that a significant pedestal height is indicative of the presence of unpolarized components in the radar return. Fig. 6 summarizes the changes in ( $f_p$ ) of the forest stands during the warm and cold days. At all the test stands, the  $f_p$  increased appreciably on the cold day, the largest change being observed in the balsam poplar stands. As mentioned earlier, this is related to a

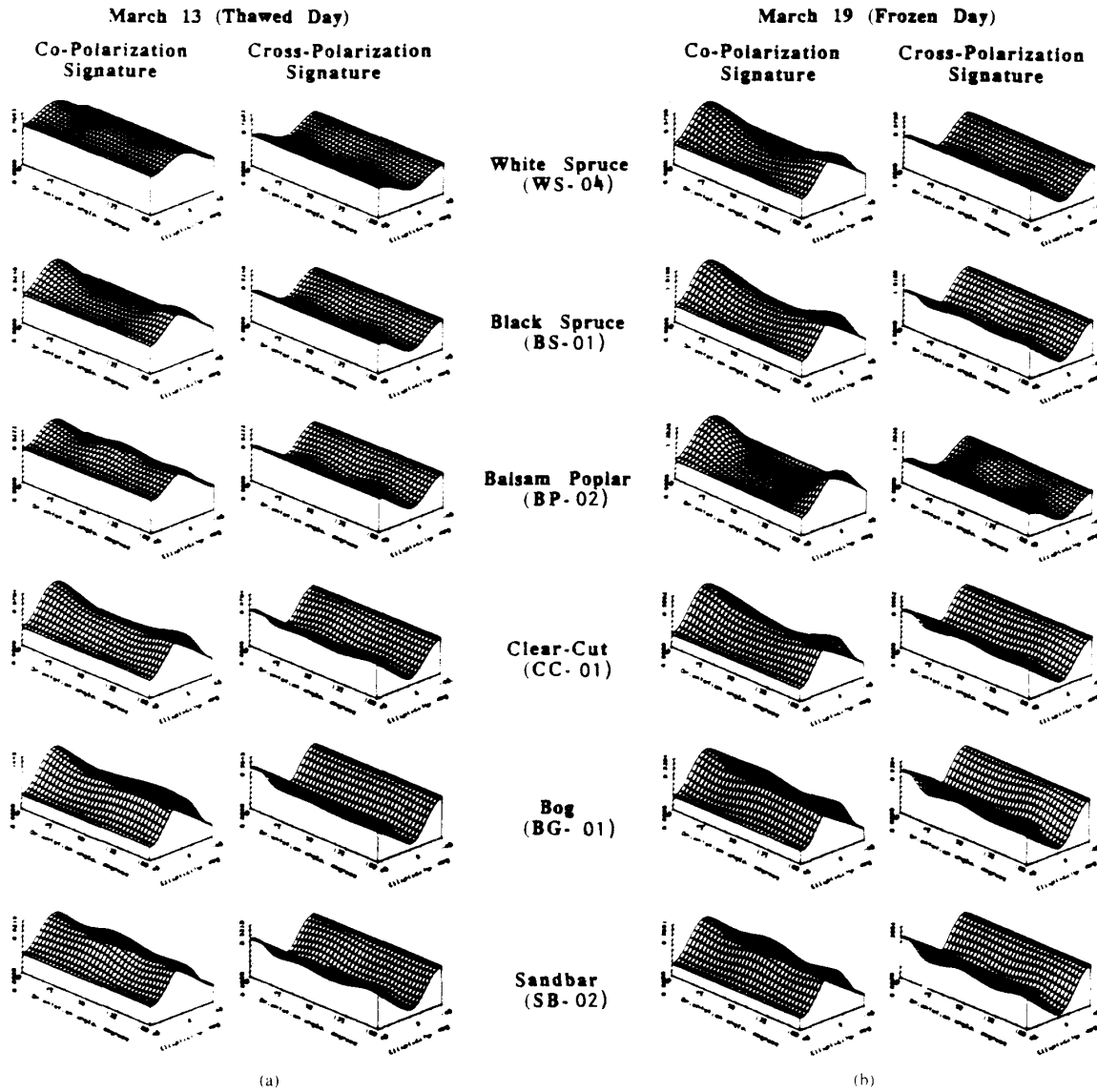


Fig. 4. Polarization signatures of sample test sites. (a) March 13. (b) March 19.

large variability in the observed scattering properties, suggesting that the scattering from the branches is more important on the warm day than on the cold day. Scattering from the clear-cut areas (dominated by single bounce scattering), on the other hand, are highly polarized with the  $f_p$  close to unity.

Besides the fractional polarization, which gives an indication of the contribution of the unpolarized component (component with randomly varying polarization) in the spatially averaged return, it is also fruitful to examine the distribution of the phase difference between the HH and VV returns ( $\phi_{H-V}$ ). The polarization phase difference

$\phi_{H-V}$  is obtained from the product

$$v_H v_V^* = A_H A_V e^{j\phi_{H-V}}$$

where  $\phi_{H-V} = \phi_H - \phi_V$  and  $\phi$ , and  $A$  are the phase and amplitudes of the H- and V- returns, respectively. A non-zero phase difference in the observed mean of  $\phi_{H-V}$  would be a consequence of [8]: 1) bistatic reflection by the trunks; 2) delay between the H- and V-polarized waves as they travel through the canopy; and 3) phase difference caused by scattering in the target. Fig. 7 shows the expected phase difference introduced by three different components of a composite scene [7]. A phase difference of

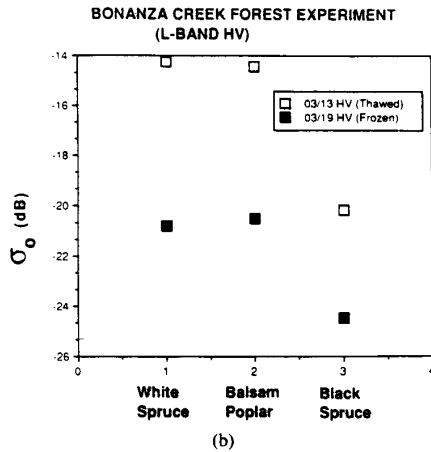
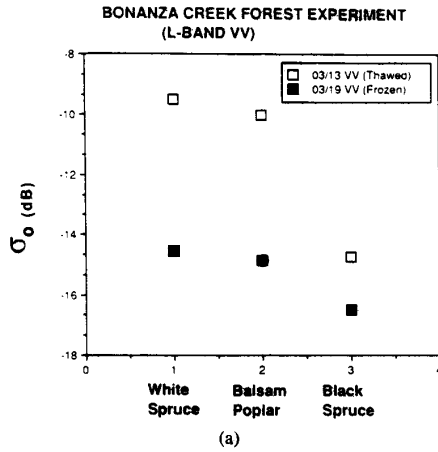


Fig. 5. Observed changes in backscatter (L-band). (a) Co-pol. (b) Cross-pol.

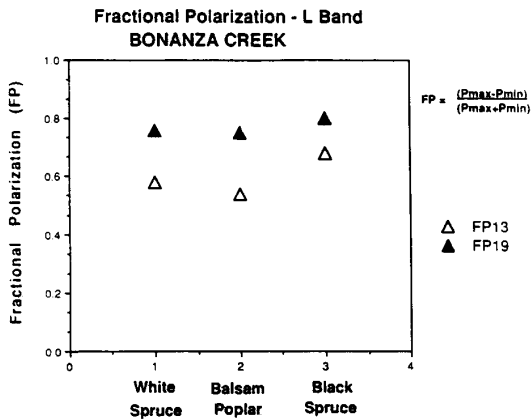


Fig. 6. Observed changes in fractional polarization (L-band).

180° is characteristic of the dominant double-bounce scattering of the radar wave while smaller but variable amount of phase difference is introduced by the canopy.

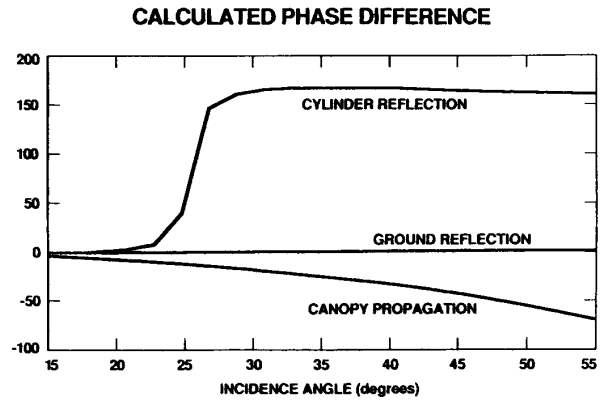


Fig. 7. Plot of the expected phase difference introduced by three different types of target at L-band (after Ulaby *et al.* [8]).

The variance of the  $\phi_{H-V}$  of a target is more related to the spatial distribution and distribution in orientation of the scatterers with respect to the transmitted polarization. A large variance in  $\phi_{H-V}$  is another indicator of large unpolarized component in the return signal [9]. Fig. 8 summarizes the changes in the mean and variance of the H-V phase difference distribution of the test stands during the warm and cold days. Sample phase difference distributions from the same test sites in Fig. 4 are shown in Fig. 9. The mean  $\phi_{H-V}$  of all test sites is not significantly different from zero and the difference in the means of the distributions between the dates is negligible. Thus the contribution of double-bounce mechanisms is not enough to introduce a significant bias in the phase difference during the conditions encountered during the two days. There are, however, observable decreases in the variance of the  $\phi_{H-V}$  distribution for all the stands, again suggesting a high variability in the scattering properties due to the contribution of branch scattering. Again, the variation in the mean phase difference is again significant compared with the calibration uncertainty provided in Table IV. There is an inverse relationship between this parameter and the  $f_p$  parameter discussed above [9]. An increase in the variance in the  $\phi_{H-V}$  generally reflects a decrease in the  $f_p$  of the average spatial return from the same target. This result again suggests the scattering from the branches is important on the warm day when contrasted with the results from the cold day.

*Scatterer Classification: L-Band*

The polarimetric L-band data from March 13 and 19 were classified into three scattering classes. The classification algorithm is based on the unsupervised classifier developed by van Zyl [10] for classification of the scattering behavior by comparing the polarization properties of each pixel in an image to that of simple classes of scattering processes such as single-bounce (odd number of reflections), double-bounce (even number of reflections),

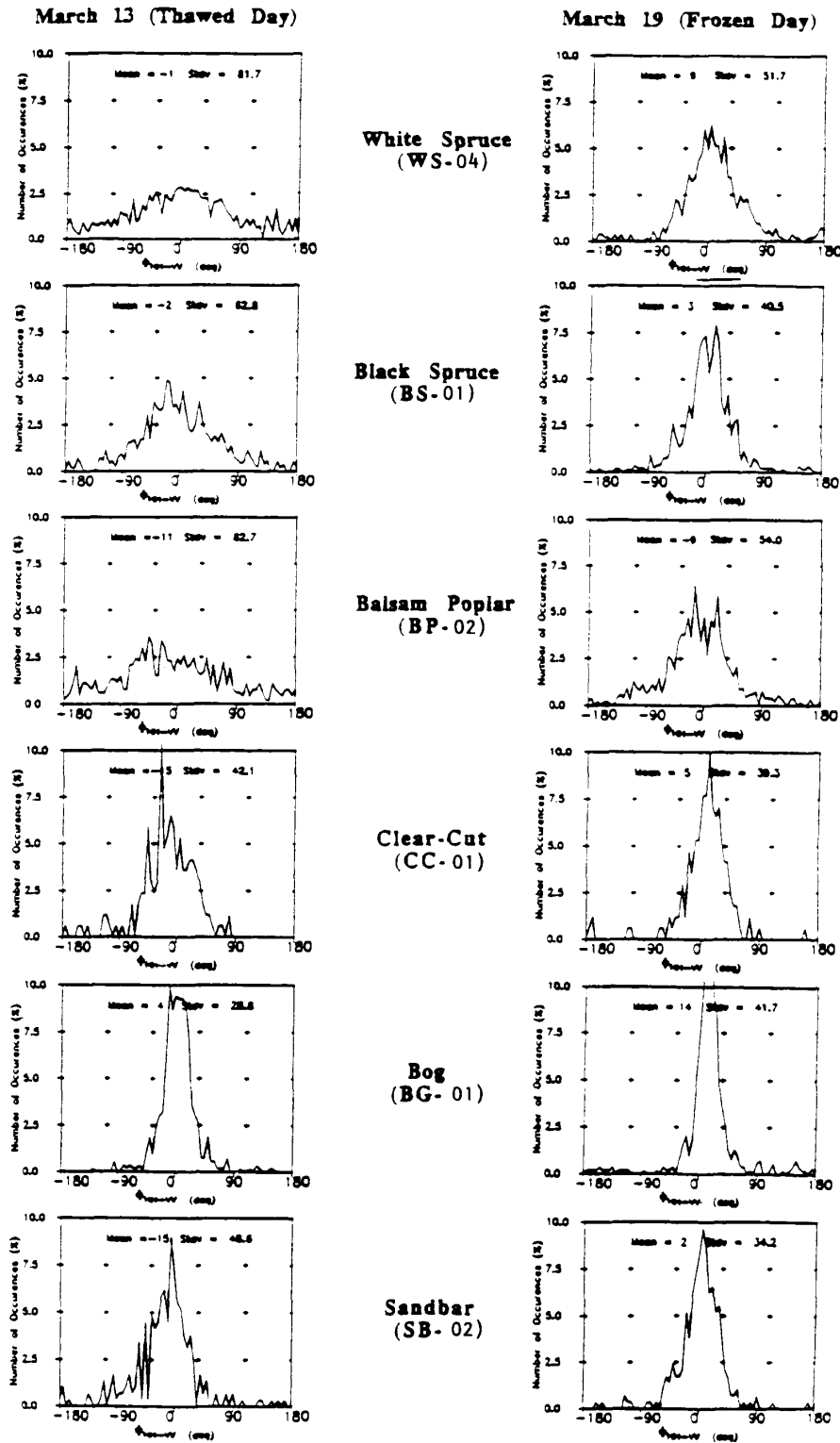


Fig. 8. Observed changes in H-V phase difference distribution: Mean and variance (L-band).

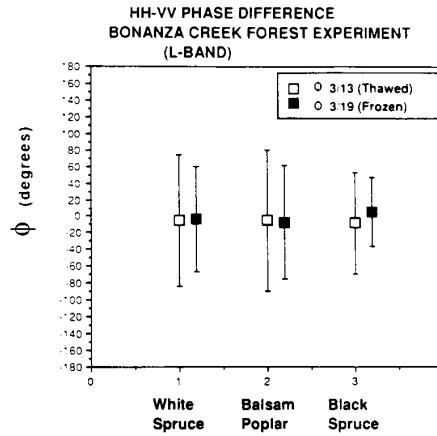


Fig. 9. Sample phase difference distribution plot for different test sites. (a) March 13. (b) March 19.

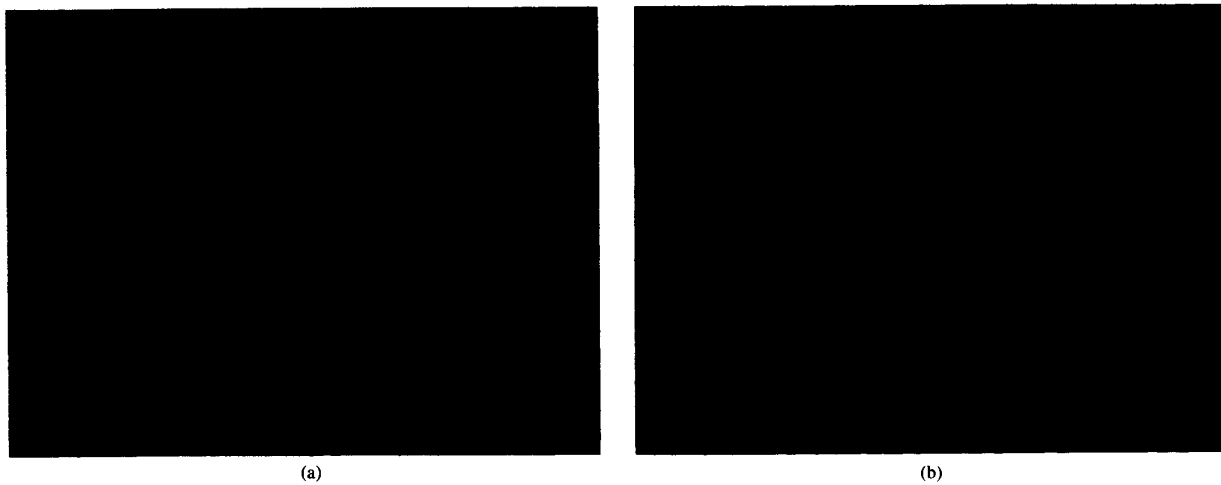


Fig. 10. Results of unsupervised scatterer classification of scattering behavior. (a) *L*-band (March 13). Pixels colored blue are areas with polarization characteristics similar to those predicted by odd number of reflections, while those colored red are areas that behave similarly to even number of reflections. Green pixels are areas that exhibit a large amount of diffuse scattering, and yellow pixels are those that do not belong to one of the three classes mentioned. (b) *L*-band (March 19).

and diffuse scattering. This technique provides a qualitative analysis of the spatial distribution of the behavior of scatterers within the image. The *L*-band classification maps generated by this algorithm are shown in Fig. 10(a) and (b).

For a forest canopy (which includes the crown, trunks, and understory), the following scattering processes which generally dominate the backscatter are 1) direct scattering (one reflection) from the top layer, ground surface, and the tree trunks; 2) double reflections from the ground surface and the tree trunks; and, 3) diffuse scattering due to multiple scattering due to contribution of the previous two mechanisms. Comparison of the classification maps from the 13 and 19 indicate a dominance of diffuse scatterers on the 13 and a dominance of single bounce scatterers on the 19. This again indicates that the scattering from the

crown is important on the thawed day whereas the single-bounce scattering from the forest canopy is important on the cold day.

Summarizing, the major component in the higher backscatter in the warm day is due to scattering from the crown. The contribution of the expected double-bounce scattering is low on both days due to the high extinction through the trunk layer on the warm day and low dielectric constants and density of trunks and branches on the cold day.

V. CONCLUSION

We have presented and compared the observed polarization signatures of selected forest stands when it is frozen and thawed. The radiometric and polarimetric measure-

U-M-I  
 DUE TO LACK OF CONTRAST, GRAPHS DID NOT REPRODUCE WELL.  
 GRAPHS FOLLOW SAME SEQUENCE AS LEGEND

ments (from the two dates) derived from the Stokes matrices were compared. Calibration of the data have shown that the changes are significant compared with the calibration uncertainties. Also, the relative contributions of different scattering mechanisms to the polarimetric behavior of the data were discussed based on these observations. Physical insights into the changes in the scattering processes were provided. The polarimetric responses of the forest were also compared to previous observations and modeling efforts. There is, in general, good agreement between the radar observations from the BCEF experiment and the expected scattering behavior. The results presented here indicate changing environmental conditions strongly affect the microwave backscatter response of forest canopies. In the L-band, the scattering behavior between the two days manifested itself in changes in the HH, VV, and HV  $\sigma_0$ 's, changes in the fractional polarization, and the changes in the variances of the H-V phase difference distributions.

#### ACKNOWLEDGMENTS

The authors wish to thank S. Durden of JPL for offering his insights in interpreting the polarimetric data and J. van Zyl for the use of his unsupervised classification software. We would also like to thank C. Slaughter, L. Viereck, B. Jaeger, J. Roth, and A. Davis for their efforts in the ground truth collection, a critical component of this experiment. We would also like to thank B. Holt, E. Kasischke, and B. Wood for their help in deploying the calibration targets.

#### REFERENCES

- [1] J. Way, J. Paris, D. Casey, F. Ahern, N. Christensen, M. C. Dobson, F. Ulaby, J. Weber, R. Hoffer, M. Imhoff, E. Kasischke, A. Milne, J. Richards, A. Sieber, P. Churchill, D. Simonett, C. Slaughter, L. Viereck, E. Mougin, and T. LeToan, "The effect of changing environmental conditions on microwave signatures of forest ecosystems," *Int. J. Remote Sensing*, vol. 11, no. 7, pp. 1119-1144, 1990.
- [2] J. Holt and A. Freeman, "Calibration of Bonanza Creek Alaska SAR imagery using along-track calibration targets," in *Proc. IGARSS*, College Park, MD, 1990, pp. 2309-2312.
- [3] M. C. Dobson, K. McDonald, F. T. Ulaby, and J. Way, "Effects of temperature on radar backscatter from boreal forests," in *Proc. IGARSS*, College Park, MD, 1990, pp. 2313-2314.
- [4] J. Klein, "Calibration of complex polarimetric SAR imaging using backscatter correlations," submitted to *IEEE Trans. Aerospa. Electron. Syst.*
- [5] P. C. Dubois and L. Norikane, "Data volume reduction for imaging radar polarimetry," in *Proc. IGARSS*, College Park, MD, 1987, pp. 1201-1203.
- [6] J. J. van Zyl, H. A. Zebker, and D. N. Held, "Imaging radar polarization signatures," *Radio Sci.*, vol. 22, pp. 529-543, 1987.
- [7] S. Durden, J. J. van Zyl, and H. A. Zebker, "Modeling and observation of radar polarization signature of forested areas," *IEEE Trans. Geosci. Remote Sensing*, vol. GE-27, no. 3, pp. 290-301, May 1989.
- [8] F. Ulaby, D. Held, M. C. Dobson, K. McDonald, and T. Senior, "Relating polarization phase difference of SAR signals to scene properties," *IEEE Trans. Geosci. Remote Sensing*, vol. GE-25, no. 1, pp. 83-92, Jan. 1987.
- [9] H. J. Eom and W.-M. Boerner, "Statistical properties of phase difference between two orthogonally-polarized SAR signals," in *Proc. IGARSS*, 1988, Edinburgh, Scotland, 1988, pp. 65-66.
- [10] J. J. van Zyl, "Unsupervised classification of scattering behavior using radar polarimetry data," *IEEE Trans. Geosci. Remote Sensing*, vol. GE-27, no. 1, pp. 36-45, Jan. 1989.
- [11] J. B. Way, E. Rignot, K. McDonald, R. Oren, R. Kwok, G. Boren, M. C. Dobson, L. Viereck, and J. E. Roth, "Evaluating type and state of Alaska Taiga forests with imaging radar for use in ecosystem flux models," *IEEE Trans. Geosci. Remote Sensing*, this issue, pp. 355-372.



**Ronald Kwok** (M'84) received the B.Sc. (summa cum laude) degree from Texas A&M University, College Station, TX, in 1976 and the Ph.D. degree from Duke University, Durham, NC, in 1980. He was a postdoctoral fellow at the University of British Columbia, Vancouver, BC, in 1981.

In 1985 he joined the Radar Science and Engineering Section at the Jet Propulsion Laboratory, Pasadena, CA, where he developed techniques for analysis of SAR imagery and served in a radar system engineering capacity on the Magellan and Alaska SAR Facility projects. He is currently Group Supervisor of the SAR Systems Development and Processing Group responsible for research and development of analysis and processing techniques for SAR data. His current interests include the application of remote sensing to the study of land and sea ice.

Dr. Kwok is a member of the American Geophysical Union, American Meteorological Society, Electromagnetics Academy, Tau Beta Pi, Phi Kappa Phi, and Eta Kappa Nu.



**Eric J. M. Rignot** (M'90) was born in Chambon sur Lignon, France. He received the Engineer's diploma from the Ecole Centrale des Arts et Manufactures Paris, in 1985, the M.S. degree in astronomy from the University of Paris VI in 1986 and the M.S. degree in aerospace engineering and in electrical engineering in 1987 and 1988, respectively, and the Ph.D. degree in electrical engineering in 1991, all from the University of Southern California.

He was employed as a Research Assistant at the University of Southern California in the Department of Aerospace Engineering from 1986-1988. He then joined the Radar Science and Engineering Section at the Jet Propulsion Laboratory, California Institute of Technology. He is a Principal Investigator on the Greenland AIRSAR Experiment, and a Co-Investigator on an ERS-1 SAR project and BOREAS. His current research interests include analysis of radar scattering from glacier facies, monitoring of environmental conditions in boreal forests using ERS-1 and J-ERS-1 SAR, and retrieval of forest parameters from polarimetric SAR data.

Dr. Rignot is a member of the AGU.



**JoBea Way** was born in Lorrain, Ohio, in 1954. She received the B.S. degree in chemistry from the University of California, Berkeley, and the M.S. and Ph.D. degrees from the California Institute of Technology in planetary sciences.

She has worked at the Jet Propulsion Laboratory since 1976 where she is the Principal Investigator of an ERS-1 Forest Project to determine the effects of canopy temporal variations on radar backscatter. This research is based in Alaska at the Bonanza Creek Experimental Forest. She is a

Team Member on the EOS SAR Facility Instrument Team and Co-Investigator with Dr. Robert Dickinson on an EOS Interdisciplinary Investigation to study global climate change. She was recently selected as a Principal Investigator for the NASA BOREAS Project to utilize SAR-derived measurements of seasonal state in carbon flux models. She has been involved in all of JPL's spaceborne SAR projects since 1981. She was the Science Coordinator for the first Shuttle Imaging Radar, SIR-A, and the Experiment Scientist for its follow-on, SIR-B. She is currently coordinating the vegetation studies for SIR-C/X-SAR and will be one of the payload communicators with the astronauts during the mission. She is the Project Scientist for the EOS SAR.



**Anthony Freeman (M'83)** received the B.Sc. (Hons.) degree in mathematics in 1979 and the Ph.D. degree in astrophysics in 1982, both from the University of Manchester Institute of Science and Technology, Manchester, England.

Between 1982 and 1987 he worked at the Marconi Research Center, Chelmsford, England, on moving target imaging with SAR, aircraft SAR motion compensation, SAR design studies, and image quality assessment. Since 1987 he has been employed by the Jet Propulsion Laboratory, Cal-

ifornia Institute of Technology, Pasadena, CA, as a Radar Systems Specialist and Group Supervisor. His current research interests are in the field of multifrequency, multipolarization SAR calibration and in classification and information extraction from SAR imagery. He is chairman of the Committee on Earth Observing Sensors (CEOS) Working Group on SAR calibration. He is a Principal Investigator on three NASA-sponsored studies: one on SIR-C calibration, one on calibration and change detection using Alaska SAR Facility ERS-1 data, and one on geographical information systems.